Single-Switch Single-Magnetic PWM Converter Integrating Voltage Equalizer for Partially-Shaded Photovoltaic Modules in Standalone Applications

Masatoshi Uno, *Member, IEEE*, and Akio Kukita

***Abstract*— To prevent partial-shading issues in photovoltaic (PV) systems, various kinds of voltage equalizers that virtually unify characteristics of shaded and unshaded modules have been proposed. Although PV string utilization can be dramatically improved, PV systems tend to be complex and costly because, in addition to the main converter for string control, voltage equalizers are separately necessary. This paper proposes the single-switch single-magnetic PWM converter integrating the voltage equalizer using the series-resonant voltage multiplier (SRVM) for standalone PV systems. By utilizing a square wave voltage generated across a filter inductor in a PWM buck converter for driving the SRVM, the main PWM converter and voltage equalizer can be integrated into a single unit with reducing the total switch and magnetic component counts, achieving not only system-level but also circuit-level simplifications. The experimental test using the prototype for three PV modules connected in series was performed emulating a partial-shading condition. The integrated converter effectively precluded the partial shading issues and significantly improved the power available at a load, demonstrating its efficacy.**

***Index Terms* — Integrated converter, partial-shading, PWM buck converter, series-resonant voltage multiplier, voltage equalizer**

I. Introduction

Partial shading on a photovoltaic (PV) string comprising multiple PV modules/substrings (hereafter simply call module) connected in series is well known to trigger major issues; not only is the power generation of the string as a whole significantly reduced but also multiple power point maxima, which hinder and confuse ordinary maximum power point tracking (MPPT) algorithms, appear on the string's P–V characteristic. The root of these issues is the mismatch in module characteristics; a shaded module that is less capable of producing current is bypassed and, therefore, its voltage is clumped to sub-zero value, even though it can potentially produce power to some extent, as shown in Fig. 1. To preclude such issues, distributed MPPT (DMPPT) systems [1], [2], where each module is individually controlled by a micro-converter or -inverter, have been conventionally used. Although partial-shading issues can be effectively prevented in DMPPT systems, PV systems tend to be complex and costly as the number of converters necessary is proportional to the number of modules.

As a powerful alternative solution, various kinds of differential power processing (DPP) converters and voltage equalizers (hereafter simply call equalizers) have been extensively researched and proposed [3]–[27]. With these converters, a fraction of generated power of unshaded modules is transferred to shaded ones so that all modules operate at the same voltage or even at each MPP. More clearly, characteristics of all modules (not only unshaded modules but also shaded ones) are virtually unified by voltage equalizers.

The most straightforward topologies are the adjacent module-to-module equalizers listed in Fig. 2. Among these, the bidirectional PWM buck-boost converters [3]–[10], shown in Fig. 2(a), and some extended PWM converter topologies [11]–[14] have been widely employed. An alternative to the bidirectional buck-boost converter is the multi-stage chopper [15], [16] that can reduce the switch count to some extent [see Fig. 2(b)]. Switched capacitor converter [see Fig. 2(c)] can also be used as a miniaturized voltage equalizer [17]–[19]. These adjacent module-to-module equalization topologies, however,

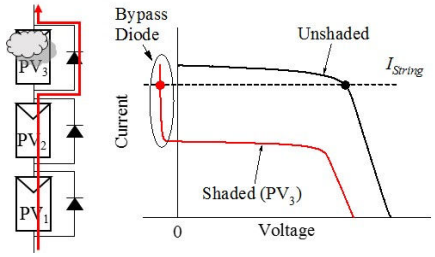

Fig. 1. Shaded and unshaded modules in a PV string.

Manuscript received December 26, 2016, revised February 7, 2017; accepted February 28, 2017. This work was supported partly by the Ministry of Education, Culture, Sports, Science, and Technology through Grant-in-Aid for Young Scientists (B) 25820118.

M. Uno is with the Faculty of Engineering, Ibaraki University, Hitachi 316-8511, Japan (e-mail: masatoshi.uno.ee@vc.ibaraki.ac.jp).

Akio Kukita is with the Institute of Space and Astronautical Science, Japan Aerospace Exploration Agency, Sagamihara 252-5210, Japan (email:kukita.akio@jaxa.jp).

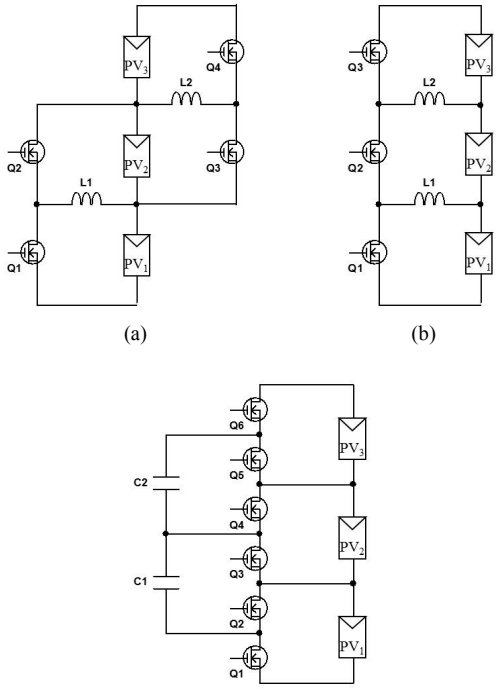

Fig. 2. Adjacent module-to-module equalizers based on (a) buck-boost converters, (b) multi-stage choppers, and (c) switched capacitor converters.

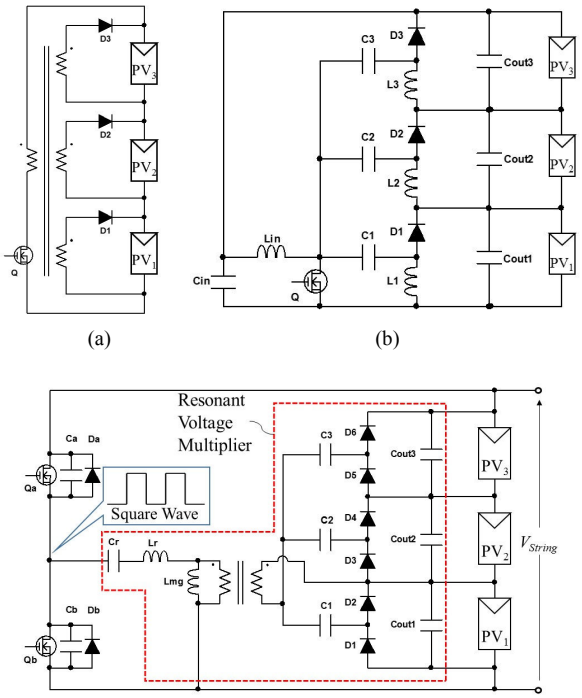

Fig. 3. String-to-module equalizer based on (a) multi-winding flyback converter, (b) multi-stacked buck-boost converters, and (c) LLC resonant voltage multiplier.

tend to increase the circuit complexity as the switch count soars with the number of modules connected in series — each switch requires several ancillary components, including a gate driver IC and its auxiliary power supply, and therefore, the switch count is a good index to represent the circuit complexity. Furthermore, since the power transfer in these topologies is limited only between adjacent modules, the power from unshaded modules may have to traverse several equalizers and modules before reaching shaded ones, collectively increasing power conversion losses.

Isolated bidirectional flyback converters provide direct power transfer paths between the string and shaded modules [20]–[23]. Although flexible equalization is feasible, these equalizers are costly and bulky because each isolated converter requires switches as well as an isolation transformer — the numbers of switches and transformers are proportional to that of PV modules connected in series.

Meanwhile, string-to-module equalizers offer simpler circuit and direct power transfer path from the string to shaded modules. Some representative topologies are listed in Fig. 3. The multi-winding flyback converter [24], shown in Fig. 3(a), is a desirable choice from the circuit simplicity viewpoint but the design difficulty of the multi-winding transformer might be a stumbling block. The single-switch equalizer using multi-stacked buck-boost converters [25], [26], shown in Fig. 3(b), is not only simple but also transformerless. However, the inductor count is proportional to the number of PV modules, likely increasing the circuit volume and cost.

The two-switch voltage equalizer using the LLC resonant voltage multiplier [27], shown in Fig. 3(c), has been proposed in the previous work. This equalizer is very simple and can be designed compact thanks to the two-switch single-magnetic topology. Furthermore, shaded modules with this equalizer can be automatically equalized even without feedback control, hence further simplifying the circuit by eliminating a feedback control loop for equalization.

The schematic diagram of the PV system using the adjacent module-to-module equalizers, isolated equalizers, and string-to-module equalizer are depicted in Figs. 4(a)–(c), respectively. PV strings in these systems can be operated without suffering from the partial-shading issues thanks to the equalizer(s). However, the main dc-dc converter for string control and the equalizer(s) to prevent partial-shading issues are separately necessary, likely increasing the system complexity and cost. This tendency is undesirable especially for standalone applications that represent small-scale PV systems where simplicity and cost reduction are of great importance. If the main dc-dc converter and equalizer(s) were to be integrated into a single unit, the PV system would be simpler and more economic.

In our previous work [28], the PWM converter integrating the voltage equalizer using the resonant voltage multiplier was proposed to simplify the system and reduce the circuit complexity. The resonant voltage multiplier highlighted in Fig. 3(c) is integrated with a PWM buck converter to reduce the total switch count. However, the PWM converter and equalizer require magnetic components separately (i.e., an inductor and transformer), which are undesirable from the perspective of circuit volume and cost. The topology proposed in [29], on the

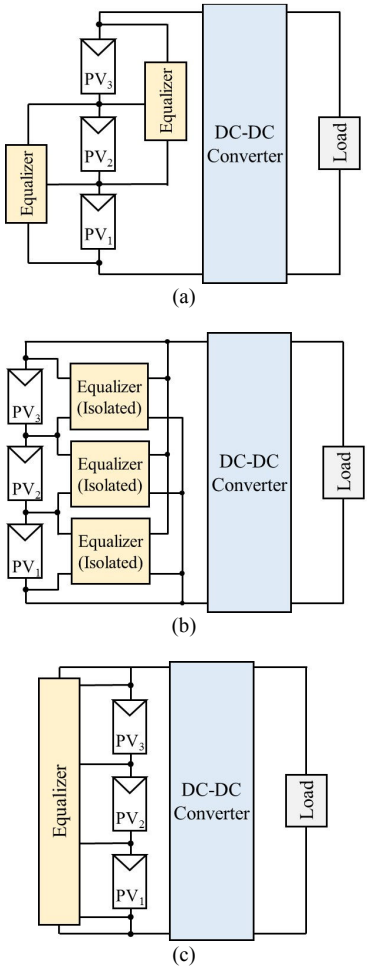

Fig. 4. Schematic diagrams of PV system using (a) adjacent module-to-module equalizers, (b) isolated equalizers, and (c) string-to-module equalizer.

other hand, not only combines the PWM converter and equalizer but also integrates the inductor and transformer, hence reducing the circuit volume.

This paper presents the extended and fully developed work about the integrated converter previously reported in [29]. The schematic diagram of the integrated converter is shown in Fig. 5. A PWM buck converter and resonant voltage multiplier can be integrated into a single unit with reducing both the switch and magnetic component counts, achieving the system- and circuit-level simplifications. Section II discusses the derivation of the proposed integrated converter and its major features. Detailed operation analysis is performed in Section III, followed by the derivation of a dc equivalent circuit that contributes to the significant reduction in simulation burden and time in Section IV. The design guideline is briefly mentioned in Section V. Experimental results will be shown in Section VI and are verified in Section VII by the simulation analysis using the derived dc equivalent circuit.

II. Integrated Converter

A. Key Elements for Integrated Converter

The proposed integrated converter is basically the combination of a traditional PWM buck converter shown in Fig. 6 and the resonant voltage multiplier emphasized in Fig. 3(c). In general, square wave voltages are generated across the switch, inductor, and diode, as shown in the inset of Fig. 6, in which only the inductor voltage v_L is depicted for the sake of clarity. Meanwhile, the resonant voltage multiplier is driven by square wave voltage produced by the leg consisting of Q_a and Q_b, as can be seen in Fig. 3(c).

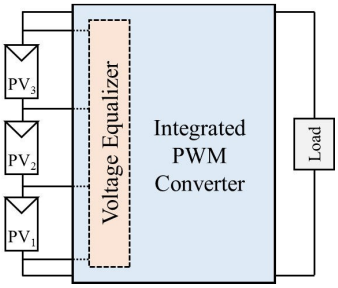

Fig. 5. Notional schematic diagrams of PV system using integrated converter.

B. Integrated Converter Topology

By utilizing the square wave voltage generated in the PWM buck converter to drive the resonant voltage multiplier, the PWM converter and voltage equalizer can be integrated into a single unit. The derived integrated converter for three PV modules connected in series is shown in Fig. 7.

In the conventional equalizer, the LLC resonant voltage multiplier was used to achieve soft switching operation but its fundamental operation is nearly identical to the series-resonant voltage multiplier (SRVM) [27]. In the derived integrated converter, however, the LLC resonant operation is no longer able to achieve soft switching because it is the main PWM buck converter that dictates the switching manner.

The PWM buck converter plays a role of string control while the SRVM performs voltage equalization for PV modules. The SRVM is driven by the square wave voltage of v_L that is automatically generated in the PWM buck converter. The number of PV modules connected in series can be arbitrary extended by adding more capacitors and diodes in the voltage multiplier — detailed discussion about the extendibility of the voltage multiplier can be found in [27]. Other PWM converters, such as boost, SEPIC, Zeta, Ćuk converters, etc., can also be used as a main converter for string control by utilizing a square wave voltage generated in each converter.

C. Major Features

Two converters (i.e., the PWM converter and equalizer) are

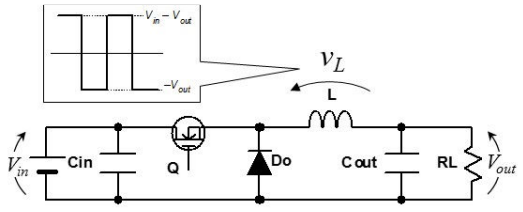

Fig. 6. Conventional PWM buck converter and its square wave voltage generated across filter inductor.

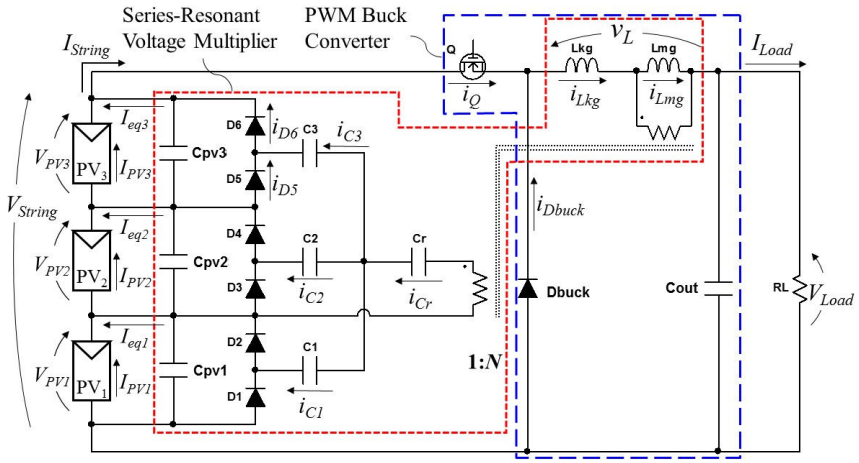

Fig. 7. Proposed integrated converter for three PV modules connected in series.

integrated into a single unit, realizing system-level simplification by reducing the converter count in the system. The SRVM is driven by the square wave voltage generated by the PWM converter and is basically switchless. The switch count in the integrated converter as a whole is only one, dramatically reducing the switch count and simplifying the circuit compared to conventional equalizers — the conventional system consisting of a PWM converter and SRVM-based equalizer, shown in Figs. 6 and 3(c), respectively, requires three switches in total. In addition, two magnetic components (an inductor and transformer) in the conventional system can also be integrated into one, reducing the circuit volume and cost.

Similar to the conventional switched capacitor-based equalizer [17], module voltages with the proposed integrated converter are simply unified, not individually controlled to be at each MPP. Individual MPPT operation (e.g., by buck-boost converters [5], [6] and multi-stage choppers [16]) undoubtedly realizes greater energy yield from PV strings at the cost of complex control techniques. However, the difference between the individual MPPT and simple voltage equalization is reportedly about 2% [22] because MPP voltages are relatively insensitive to shading conditions compared to currents [17], [22]. Hence, equalizing module voltages simply by the proposed integrated converter would be beneficial enough for modules to operate at each near-MPP.

The major drawback of the proposed integrated converter is that the performance of the voltage equalizer cannot be optimized because of the integration, as will be detailed in Section IV-B. Therefore, the proposed integrated converter is best suitable for relatively small power applications, such as standalone PV systems, where system simplicity and cost reduction are prioritized.

III. Operating Analysis

A. Fundamental Operation

Key operation waveforms as well as current flow directions when PV_3 is partially-shaded are shown in Figs. 8 and 9, respectively. Current flow paths in the voltage multiplier in Fig. 9 are illustrated by supposing that currents flowing in the voltage multiplier are completely buffered by smoothing capacitors C_{pv1}–C_{pv3}.

Mode 1 [Fig. 9(a)]: As the switch Q is turned on, Mode 1 begins, and the current of the transformer's magnetizing inductance i_{Lmg} starts linearly increasing. The voltage across the primary winding v_L is equal to $V_{String} - V_{Load}$, by which the SRVM is driven. As $V_{String} - V_{Load}$ is applied to the primary winding, the resonant capacitor C_r on the secondary winding and the leakage inductance L_{kg} starts resonating, and sinusoidal resonant current i_{Cr} flows through C_3 and D_6 in the voltage multiplier. Hence, the switch current i_Q as well as the leakage inductance current i_{Lkg} are equivalent to i_{Lmg} with i_{Cr} superimposed on it. As i_{Cr} reaches zero, the operation moves to the next mode.

Mode 2 [Fig. 9(b)]: No current flows on the transformer secondary side while i_{Lmg} is still linearly increasing. In other words, the voltage equalizer (i.e., the SRVM) is essentially inactive in this period, and therefore, this operation mode is identical to the on-period of traditional PWM buck converters.

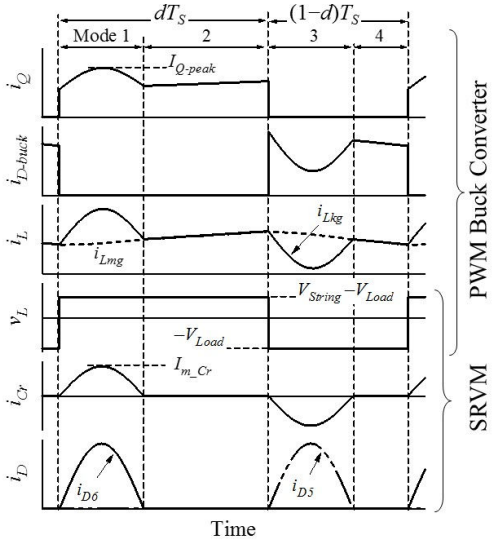

Fig. 8. Key operation waveforms when PV_3 is shaded.

Mode 3 [Fig. 9(c)]: This operation mode begins as Q is turned off. Similar to traditional buck converters, i_{Lmg} is commutated to the free-wheeling diode D_{buck}. As D_{buck} starts conducting, v_L drops to $-V_{Load}$, and the sinusoidal resonant current of i_{Cr} flows in the opposite direction as that in Mode 1. Hence, the current of D_{buck}, i_{Dbuck}, is equal to i_{Lmg} with the reflected i_{Cr} superimposed on it. The current flow direction on the secondary side is also opposite to that in Mode 1; i_{Cr} flows through C_3 and D_5. Mode 3 ends when i_{Cr} reaches zero.

Mode 4 [Fig. 9(d)]: Similar to Mode 2, the SRVM is basically inactive, and therefore, Mode 4 is essentially identical to the off-period of traditional PWM buck converters.

Overall, the sinusoidal resonant current of i_{Cr} flows as v_L swings. Meanwhile, the even- and odd-numbered diodes that are connected in parallel with the shaded module PV_3 (D_6 and D_5 in Fig. 7) alternately conduct. Since an average current of capacitors under steady-state conditions must be zero, the average current of diodes (D_5 and D_6) flows toward the shaded module PV_3 in the form of equalization current. The automatic equalization mechanism by the voltage multiplier will be explained in detail in Section IV-A.

B. PWM Buck Converter

The operation of the PWM buck converter in the proposed integrated converter is basically identical to that of traditional buck converters, except for the current superposition found in Modes 1 and 3. Similar to the traditional buck converter, i_{Lmg} increases and decreases with slopes of $(V_{String} - V_{Load})/L_{mg}$ and $(-V_{Load}/L_{mg})$ during on- and off-periods, respectively (where V_{Load} is the load voltage, as designated in Fig. 7). Therefore, from the volt-second balance on L_{mg}, the voltage conversion ratio is given by

$$V_{Load} = dV_{String}, \tag{1}$$

where d is the duty cycle of Q.

As can be seen in Fig. 9, the SRVM is active only in Modes 1 and 3. Meanwhile, according to (1), d varies with V_{String} that is dependent on various conditions, such as irradiation, temperature, and current drawn. In order for the SRVM's operation to be independent on the duty cycle variation, Modes 2 and 4 should exist to buffer the duty cycle variation.

The lengths of Modes 1 and 3 are determined by the resonant period T_r given by

$$T_r = \frac{1}{f_r} = \frac{1}{2\pi\sqrt{L_{kg}\dfrac{C_r}{N^2}}}, \tag{2}$$

where f_r is the resonant frequency, and N is the transformer turn ratio. In order for Modes 2 and 4 to exist, half the resonant period $T_r/2$ must be shorter than dT_S and $(1-d)T_S$ (T_S being the switching period). From this relationship, the following criterion is yielded;

$$1 - \frac{f_S}{2f_r} > d > \frac{f_S}{2f_r}, \tag{3}$$

where f_S is the switching frequency. This equation suggests that f_S/f_r should be determined considering the variation range of d in practical use.

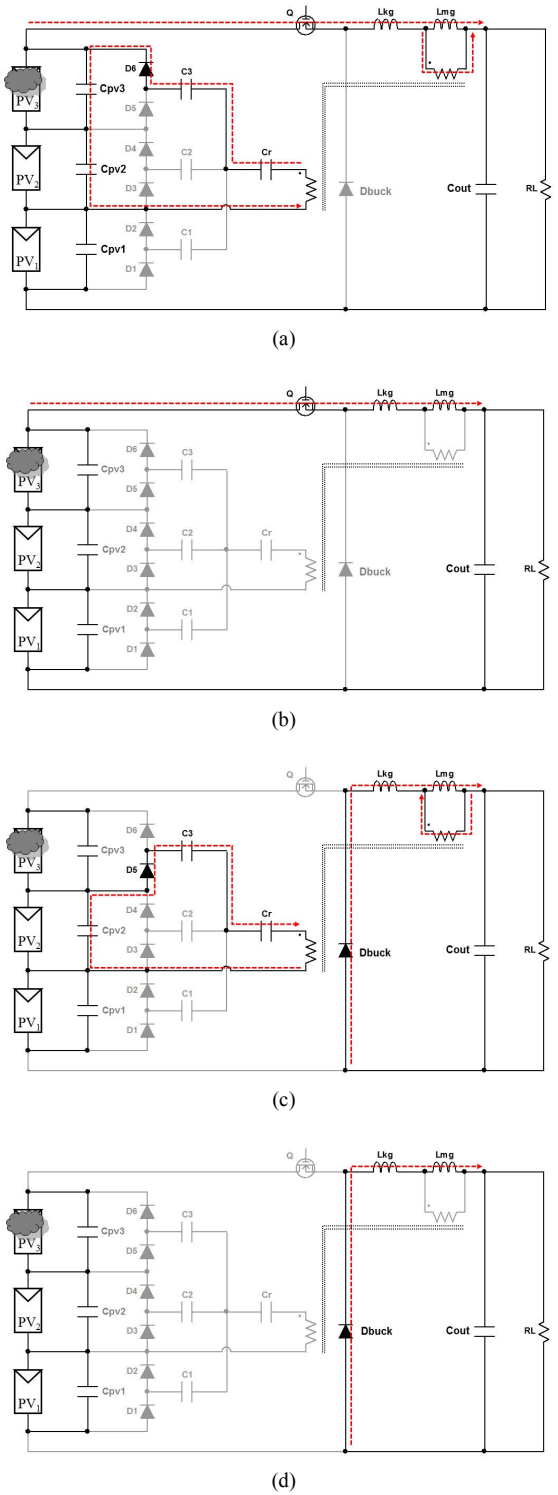

Fig. 9. Operation modes when PV_3 is shaded: (a) Mode 1, (b) Mode 2, (c) Mode 3, (d) Mode 4.

C. Series-Resonant Voltage Multiplier (SRVM)

As mentioned in the previous subsection, the SRVM is active only during Modes 1 and 3. Neglecting the inactive periods of Modes 2 and 4 considerably simplifies the analysis; the SRVM can be assumed to be driven by square wave voltage with 50%

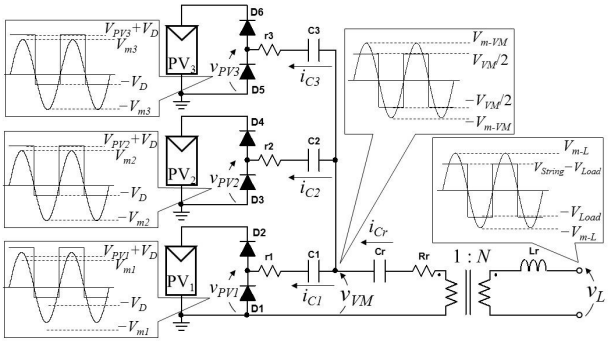

Fig. 10. Equivalent circuit of SRVM.

duty cycle. In addition, since capacitors C_1–C_3 in the voltage multiplier can be regarded as coupling capacitors, which allow ac components only to flow through, PV_1–PV_3 can be equivalently separated and grounded, yielding the equivalent circuit shown in Fig. 10. v_{VM} is the input voltage of the voltage multiplier, and v_{PV1}–v_{PV3} are the voltages of lower diodes connected in parallel with PV_1–PV_3.

From the fundamental harmonics approximation based on Fourier Series, square wave voltages of v_L, v_{VM}, and v_{PVi} (i = 1…3) can be approximated as sinusoidal waves with amplitudes of V_{m_L}, V_{m_VM}, and V_{m_PVi}, as

$$\begin{cases} v_L = V_{m\_L}\sin\omega_r t = \dfrac{2}{\pi}V_{String}\sin\omega_r t \\ v_{VM} = V_{m\_VM}\sin\omega_r t = \dfrac{2}{\pi}V_{VM}\sin\omega_r t \\ v_{PVi} = V_{m\_PVi}\sin\omega_r t = \dfrac{2}{\pi}\left(V_{PVi}+2V_D\right)\sin\omega_r t \end{cases}, \tag{4}$$

where V_{VM} is the peak-to-peak voltage of v_{VM}, V_{PVi} is the voltage of PV_i, V_D is the forward voltage drop of diodes, and ω_r (= $2\pi f_r$) is the angular resonant frequency. From (4), current amplitudes of i_{Cr} and i_{Ci}, I_{m_Cr} and I_{m_Ci}, can be yielded as

$$\begin{cases} I_{m\_Cr} = \dfrac{\frac{1}{N}V_{m\_L}-V_{m\_VM}}{|Z_r|} = \dfrac{2}{\pi}\dfrac{\frac{1}{N}V_{String}-V_{VM}}{R_r} \\ I_{m\_Ci} = \dfrac{V_{m\_VM}-V_{m\_PVi}}{\sqrt{r_i^2+\left(\frac{1}{\omega_r C_i}\right)^2}} = \dfrac{2}{\pi}\dfrac{V_{VM}-\left(V_{PVi}+2V_D\right)}{\sqrt{r_i^2+\left(\frac{1}{\omega_r C_i}\right)^2}} \end{cases}, \tag{5}$$

where Z_r is the characteristic impedance of the resonant tank, R_r is the resistive component of the resonant tank, and r_i and C_i are the ESR and capacitance of C_i, respectively.

The average currents flowing over C_r and C_i, I_{Cr} and I_{Ci}, are expressed as

$$\begin{cases} I_{Cr} = \dfrac{1}{T_S}\int_0^{0.5T_r} I_{m\_Cr}\sin\omega_r t dt = \dfrac{\omega_S}{\omega_r}\dfrac{I_{m\_Cr}}{\pi} \\ I_{Ci} = \dfrac{1}{T_S}\int_0^{0.5T_r} I_{m\_Ci}\sin\omega_r t dt = \dfrac{\omega_S}{\omega_r}\dfrac{I_{m\_Ci}}{\pi} \end{cases}, \tag{6}$$

where ω_S is the angular switching frequency. Substitution of (5) into (6) produces

$$\begin{cases} V_{String}-NV_{VM} = NI_{Cr}\dfrac{\omega_r}{\omega_S}\dfrac{\pi^2}{2}R_r \\ V_{VM}-\left(V_{PVi}+2V_D\right) = I_{Ci}\dfrac{\pi^2}{2}\dfrac{\omega_r}{\omega_S}\sqrt{r_i^2+\left(\dfrac{1}{\omega_r C_i}\right)^2} \end{cases}. \tag{7}$$

Simplifying (7) leads to

$$\begin{cases} V_{String}-NV_{VM} = \dfrac{I_{Cr}}{N}R_{res} \\ V_{VM}-\left(V_{PVi}+2V_D\right) = I_{Ci}R_{eqi} \end{cases}, \tag{8}$$

where

$$\begin{cases} R_{res} = \dfrac{\omega_r}{\omega_S}\dfrac{\pi^2}{2}R_r \\ R_{eqi} = \dfrac{\pi^2}{2}\dfrac{\omega_r}{\omega_S}\sqrt{r_i^2+\left(\dfrac{1}{\omega_r C_i}\right)^2} \end{cases}. \tag{9}$$

IV. Derivation of DC Equivalent Circuit

A. Series-Resonant Voltage Multiplier (SRVM)

A dc equivalent circuit of the SRVM can be derived from (8), as shown in Fig. 11. All the three PV modules are connected to the secondary winding of the ideal transformer through respective equivalent resistor R_{eqi} (i = 1…3) and two diodes. The PV string supplies the input current for the SRVM in the form of I_{Cr}/N, whereupon its reflected current I_{Cr} on the secondary side is distributed to modules as equalization currents in the form of I_{Ci}. Since all modules are tied to the common terminal of the secondary winding, I_{Cr} preferentially flows toward a shaded module whose voltage tends to be lower than that of unshaded modules (see Fig. 1), hence achieving the automatic equalization.

B. Integrated Converter as a Whole

The dc equivalent circuit shown in Fig. 11 can be redrawn by introducing an ideal multi-winding transformer that allows PV modules to be connected in series. The dc equivalent circuit of the integrated converter as a whole is shown in Fig. 12, in which the PWM buck converter is expressed as an ideal transformer with the turn ratio of 1:d.

This derived dc equivalent circuit provides an intuitive understanding of how modules operate with the proposed integrated converter. A fraction of I_{String} is supplied to the SRVM's input as I_{Cr}/N, and its reflected current is distributed to

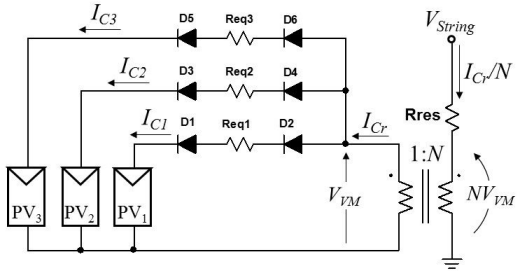

Fig. 11. DC equivalent circuit of SRVM.

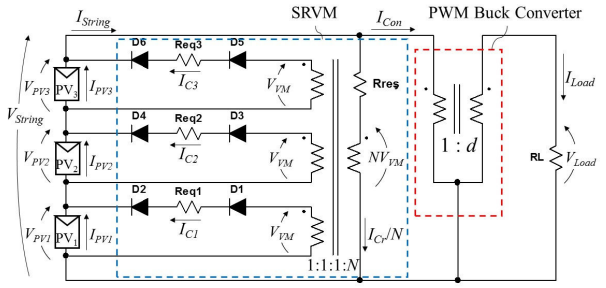

Fig. 12. DC equivalent circuit of integrated converter.

shaded module(s) as equalization current of I_{Ci}. Therefore, the SRVM operates as a power circulator that redistributes power from the string to shaded module(s). I_{String} is equal to the sum of I_{PVi} and I_{Ci} (I_{PVi} being the generated current of PV_i), and therefore, the apparent string power $P_{String} = V_{String} \times I_{String}$ is greater than the substantially-available power of $V_{String} \times I_{Con}$ (I_{Con} being the substantial input current for the PWM buck converter, as designated in Fig. 12). In other words, the power available at the load P_{Load} is $V_{String} \times I_{Con}$ in the ideal case supposing there is no loss in the PWM buck converter.

The simulation burden and time can be significantly reduced with the derived dc equivalent circuit that contains no high-frequency switching devices. Simulation analysis for MPPT is usually lengthy and very time-consuming because converters operate at switching frequencies higher than several tens kilohertz, whereas sampling intervals for MPPT range from several tens to hundreds milliseconds. In other words, there is a huge gap between switching period and sampling interval, and therefore, simulation needs to be performed at high frequency for a long stretch of time, resulting in increased simulation burden and time. Meanwhile, simulation for MPPT using the derived dc equivalent circuit can be completed in an instant because of no high-frequency switching device.

According to the comparison between Figs. 7 and 12, the equalization current for PV_i, I_{eqi}, is equal to I_{Ci};

$$I_{eqi} = I_{Ci}. \tag{10}$$

From the dc equivalent circuit, the relationship between V_{String} and V_{PVi}, and I_{Cr} and I_{Ci} can be yielded as

$$V_{String} - \frac{I_{Cr}}{N} R_{res} = N\left(V_{PVi} + 2V_D + I_{Ci} R_{eqi}\right), \tag{11}$$

$$V_{String} = \sum_{i=1}^{3} V_{PVi}, \tag{12}$$

$$I_{Cr} = \sum_{i=1}^{3} I_{Ci}. \tag{13}$$

From (11) and (13), the equivalent output resistance of the SRVM, $R_{eq\text{-}out}$, can be expressed as

$$R_{eq-out} = -\frac{\partial V_{PVi}}{\partial I_{Ci}} = \frac{R_{res}}{N^2} + R_{eqi}. \tag{14}$$

According to the equivalent circuit shown in Fig. 12, equalization currents for shaded modules flow through R_{res} and R_{eqi}. Voltages of shaded modules tend to be lower than those of unshaded ones due to voltage drops across R_{res} and R_{eqi}. In other words, the lower the value of R_{res} and R_{eqi}, the better will be the equalization performance by decreasing the voltage drop across R_{res} and R_{eqi} in the form of $(I_{Cr}/N) \times R_{res}$ and $I_{Ci} \times R_{eqi}$. This implies that module voltages can be adequately unified if voltage drops across R_{res} and R_{eqi} are sufficiently small compared to module voltages. To this end, the converter should be designed so that the values of R_{res} and R_{eqi} are adequately small.

Equation (9) suggests the reduction in ω_r/ω_S is the key to decreasing the values of R_{res} and R_{eqi}. It is equivalent to shorten the inactive periods of Modes 2 and 4. However, shortening Modes 2 and 4 leads to narrow the allowable duty cycle variation range according to (3). Hence, ω_r/ω_S should be designed to be as low as possible in the given duty cycle variation range.

V. Design Guideline

The proposed integrated converter can be designed identically to the traditional PWM converter and resonant voltage equalizer [27], except for the switch Q and transformer. Hence, this section focuses only on the switch Q and transformer.

A. Switch

As shown in Fig. 8, i_Q is equal to i_{Lkg} during the on period of Modes 1 and 2. In addition to the triangular current of i_{Lmg}, the reflected resonant current i_{Cr}/N is superimposed and flows through Q. Hence, the current rating of Q should be determined considering the superposition of the reflected resonant current.

The average current of i_{Lkg} is equal to the load current I_{Load}. Assuming all module voltages are completely equalized to be VPV and all the generated power is available at the load, I_{Load} is expressed as

$$I_{Load} = \frac{1}{V_{Load}} \sum_{i=1}^{3} V_{PV} I_{PVi}, \tag{15}$$

where I_{PVi} is the generated current of PV_i, as designated in Figs. 7 and 12. From (6) and (13), the amplitude of i_{Cr}, I_{m_Cr}, is

$$I_{m\_Cr} = \sum_{i=1}^{3} \frac{\pi \omega_r}{N \omega_S} I_{Ci}. \tag{16}$$

The peak of i_Q, $I_{Q\text{-}peak}$, is the sum of I_{Load} and I_{m_Cr} reflected on the primary side, and therefore,

$$I_{Q-peak} = I_{Load} + \frac{1}{N} I_{m\_Cr} = \sum_{i=1}^{3} \left(\frac{V_{PV} I_{PVi}}{V_{Load}} + \frac{\pi \omega_r}{N \omega_S} I_{Ci} \right). \tag{17}$$

The switch Q should be properly chosen so that its current rating satisfies the peak current expressed by (17).

The Joule loss of the switch increases due to the superposition of the reflected resonant current i_{Cr}/N, whereas the diode conduction loss is reduced, as can be seen in Fig. 7. In general, in PWM converters for low power applications such as standalone PV systems, the most dominant loss factor is the diode conduction loss. Hence, the power conversion loss of the PWM converter alone is reduced to some extent by the superposition of i_{Cr}/N.

B. Transformer

Under fully unshaded conditions, the SRVM should supply no equalization current for PV modules, meaning $I_{Ci} = 0$ and

$I_{Cr}/N = 0$ in Fig. 12. To this end, the transformer's turn ratio N needs to be properly determined. Applying $I_{Ci} = 0$ and $I_{Cr}/N = 0$ into (11) yields

$$N \geq \frac{V_{String}}{V_{PVi} + 2V_D}. \quad (18)$$

As discussed in Section II, both L_{kg} and L_{mg} of the transformer are utilized in the proposed integrated converter. Especially, L_{kg} is an important parameter that determines f_r and allowable duty cycle variation range [see (2) and (3)]. A loosely-coupled transformer that is conventionally employed for LLC resonant converters [30] would be suitable to obtain desirable inductance for L_{kg}. Although the value of L_{kg} cannot be precisely designed, f_r can be flexibly adjusted by properly choosing C_r.

VI. Experimental Results

A. Prototype

A 75-W prototype of the proposed integrated converter was designed and built for a standalone PV system comprising a 72-cell PV panel (containing three substrings) and 16-V battery as a load, as shown in Fig. 13. Component values are listed in Table I. For the prototype with the resonant frequency f_r of 230 kHz, the switching frequency f_S was determined to be 130 kHz to fulfill (3) in the duty cycle variation range between 30% and 70%. The measured power conversion efficiency of the prototype under no-shading condition was as high as 94% at the output power of 75 W.

B. Output Characteristic of SRVM

Before the equalization tests emulating partial-shading conditions, fundamental characteristics of the SRVM alone was investigated using the experimental setup shown in Fig. 14. The

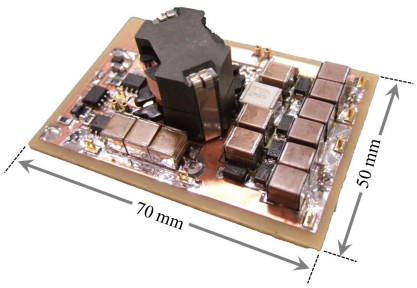

Fig. 13. Photograph of prototype.

TABLE I
Component Values

Component	Value
C_1–C_3	Ceramic Capacitor, 47 µF
C_{cv1}–C_{cv3}	Ceramic Capacitor, 100 µF × 2
D_1–D_6	Schottky Diode, RSX501L-20, V_D = 0.47 V
C_r	Film Capacitor, 1 µF × 2
Transformer	N_1:N_2 = 14:5, L_{kg} = 1.9 µH, L_{mg} = 66 µH
Q	FDS86240, R_{on} = 35.3 mΩ
D_{buck}	Schottky Diode, D3FJ10, V_D = 0.74 V
C_{out}	Ceramic Capacitor, 100 µF × 3

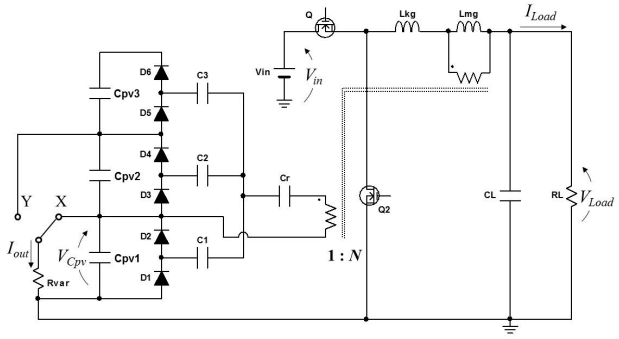

Fig. 14. Experimental setup for characteristic measurement.

integrated converter was powered by a voltage source V_{in} instead of PV modules. Meanwhile, a variable resistor R_{var} was connected through the selectable tap, with which current flow paths under partial-shading conditions can be emulated. Selecting the tap X emulates the case that PV_1 is shaded. With the tap Y, on the other hands, the SRVM operates as if PV_1 and PV_2 are equally shaded while PV_3 is unshaded. The measurement was carried out at fixed duty cycles of d = 30, 50, and 70% with I_{Load} = 0 or 4.0 A.

The measured output characteristics of the SRVM are shown in Fig. 15. As the output current of the SRVM, I_{out}, increased, the voltage of C_{pv1}, V_{Cpv}, linearly declined. The measured output characteristics were independent on d, verifying the duty-independent resistance characteristic, as expressed by (9) and (14). The values of $R_{eq\text{-}out}$ under one- and two-module-shaded conditions (i.e., Tap X and Y in Fig. 14) were determined to be 0.8 and 1.2 Ω, respectively. By applying these $R_{eq\text{-}out}$ values into (14), R_{eqi} and R_{res} were calculated to be 0.4 and 3.1 Ω, respectively. The power conversion efficiencies of the SRVM were also measured when I_{Load} = 0 A, as shown in the top panel of Fig. 15. The measured efficiencies proportionally decreased with V_{Cpv}. The results suggest that the

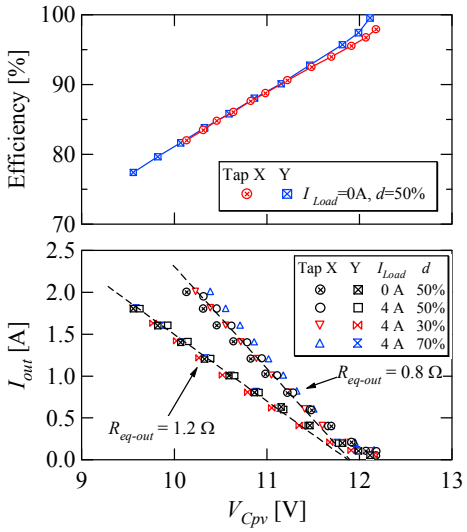

Fig. 15. Measured output characteristics of SRVM of the integrated converter.

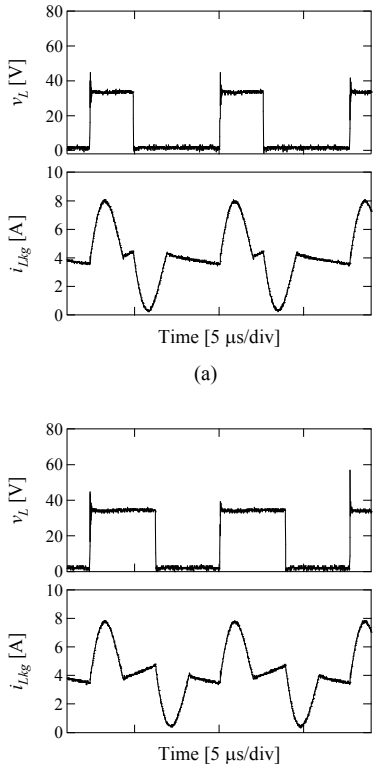

Fig. 16. Measured waveforms when Tap X was selected and I_{Load} = 4.0 A and I_{out} = 2.0 A with (a) d = 30% and (b) d = 50%.

key to improving the SRVM's efficiency is the reduction in $R_{eq\text{-}out}$ so that V_{Cpv} does not decline much.

The measured key waveforms when Tap X was selected and I_{Load} = 4.0 A and I_{out} = 2.0 A with d = 30% and 50% during the characteristic measurement are shown in Figs. 16(a) and (b), respectively. As v_L swung, sinusoidal resonant current was superimposed on the triangular current wave, very similar to the theoretical waveforms shown in Fig. 8.

C. Equalization

The experimental equalization test emulating a partial-shading condition was performed using solar array simulators (E4360A, Agilent Technologies). Individual PV module characteristics used for the equalization test are shown in Fig. 17(a); PV_1 and PV_2 were unshaded while PV_3 was shaded and its short-circuit current was half that of the others. Maximum powers of unshaded and shaded modules were 22.8 W and 10.1 W, respectively, and hence, the string was ideally capable of generating 55.7 W. A constant-voltage load of V_{Load} = 16 V was connected to the output of the integrated converter, and d was manually varied in order to sweep the string characteristics. String characteristics without equalization for comparison were also measured by directly connecting a variable resistor to the string.

Measured string characteristics with/without equalization are shown and compared in Fig. 17(b). There were two power point maxima when without equalization, and the global maximum

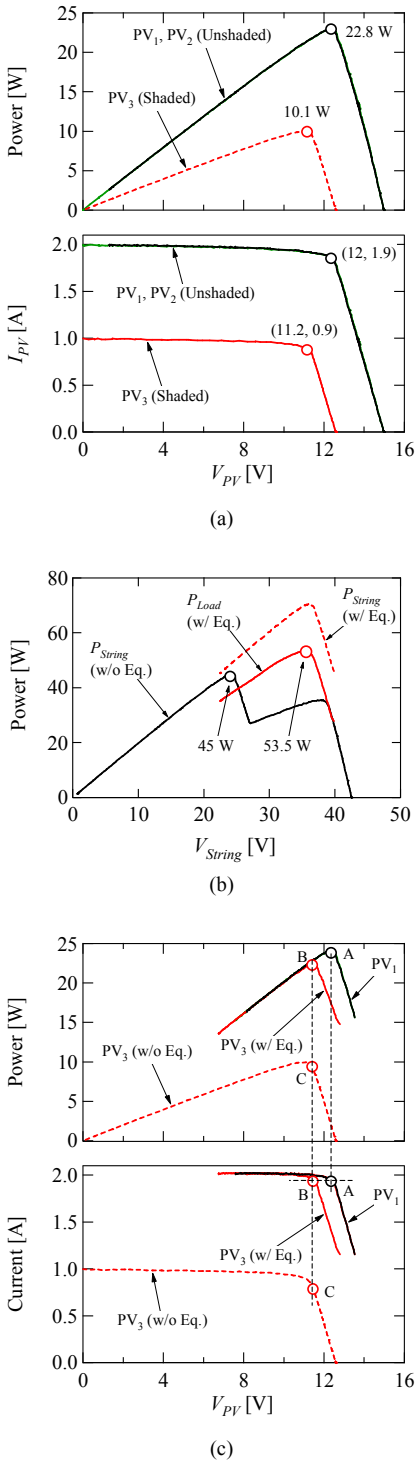

Fig. 17. Experimental results of equalization test: (a) Individual PV module characteristics used for the experiment, (b) string characteristics with/without equalization, (c) individual module characteristics with equalization.

power was merely 45 W at V_{String} = 24 V. With the equalization by the integrated converter, on the other hand, the local MPP successfully disappeared. The apparent power at the string, P_{String}, was greater than the power available at the load P_{Load}, as discussed in Section IV-B, and the gap between P_{String} and P_{Load} corresponds to the power inputted to the SRVM. The maximum

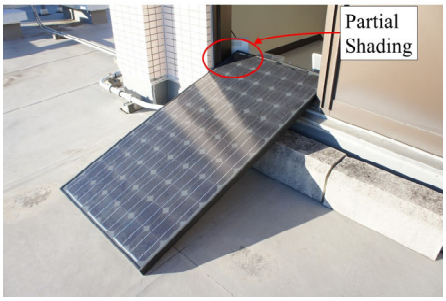

Fig. 18. Experimental setup for equalization test using real PV panel.

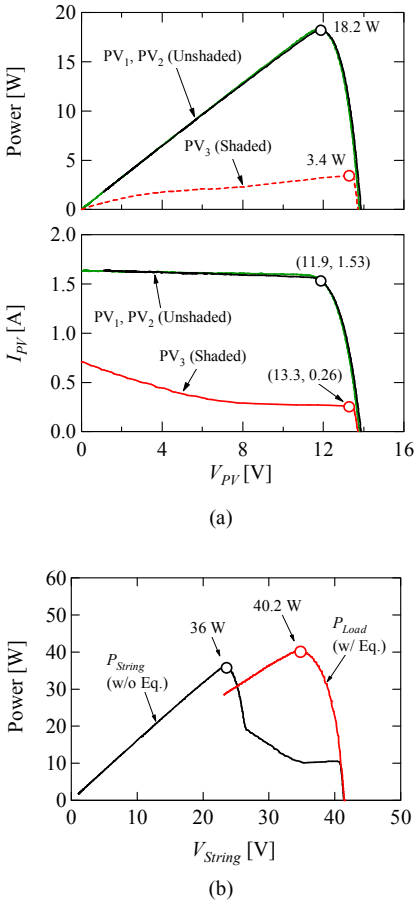

Fig. 19. Experimental results of equalization test for real PV panel: (a) Individual module characteristics used for the experiment, (b) string characteristics with/without equalization.

power of P_{Load} was as high as 53.5 W at V_{String} = 36 V, indicating that 96% of the string power was available at the load when with the integrated converter.

Individual module characteristics during the equalization test were also measured, as shown in Fig. 17(c). The characteristics of PV_3 without equalization are also graphed with dashed lines as reference. Meanwhile, characteristics of PV_1 and PV_2, the unshaded modules, with and without equalization were identical, and therefore, the characteristics of PV_1 only were displayed for the sake of clarity. When the string current was 1.9 A, for example, the unshaded module PV_1 operated at the points A, its MPP. Since all the modules in the string provide the same current, the operating points on the virtual characteristics of PV_3 (PV_3 w/Eq.) are determined to be B. The actual operating points of PV_3 must be at the same voltage as B, and hence, points C are determined. The current difference between B and C corresponds to the equalization current supplied for PV_3. The operating voltage of PV_3 (i.e., B and C) was slightly lower than that of PV_1 (point A), and (11) accounts for this voltage gap — a shaded module voltage is lower than that of unshaded ones due to the voltage drop across R_{eq3} and R_{res} in the dc equivalent circuit shown in Fig. 12, as discussed in Section IV-B. In other words, these operation points can also be determined with the dc equivalent circuit shown in Fig. 12 and (10), as will be verified in the next section.

D. Equalization for Real PV Panel

The equalization test for the real 72-cell PV panel was performed using the prototype. The characteristics of the PV panel with and without the integrated converter were measured at 15:25 in the evening in February 2017, in Hitachi, Japan. The experimental setup is shown in Fig. 18. The PV panel was placed so that one of three modules was intentionally partially-shaded. The measured individual module characteristics are shown in Fig. 19(a). The characteristic of the shaded module PV_3 was somewhat elusive, and its current at its MPP was rather lower than that of unshaded modules.

The measured string characteristics with/without the integrated converter are shown and compared in Fig. 19(b). Similar to the experimental results for the solar array simulators [see Fig. 17(b)], the local MPP vanished thanks to the equalization. The results demonstrated the practical efficacy of the proposed integrated converter.

VII. Simulation Results

To verify the derived dc equivalent circuit shown in Fig. 12, the simulation-based equalization test was also performed under the same condition as the experiment using the solar array simulators. The determined values of R_{eqi} and R_{res} of 0.4 and 3.1 Ω, respectively, in the experiment, as discusses in Section VI-B, were applied in the dc equivalent circuit for the simulation analysis. PV module characteristics were emulated using single-diode models [31]; individual PV module characteristics used for the simulation analysis are shown in Fig. 20(a).

The simulation results of the equalization test are shown in Figs. 20(b) and (c). Both the string and individual module characteristics in the simulation analysis were in good agreement with those in the experiment [see Figs. 17(b) and (c)], demonstrating that the derived dc equivalent circuit adequately represents the characteristics of the original circuit shown in Fig. 7.

VIII. Conclusions

The single-switch single-magnetic PWM converter integrating the voltage equalizer using the SRVM has been proposed for PV strings under partial shading. The proposed integrated converter can be derived from the combination of a

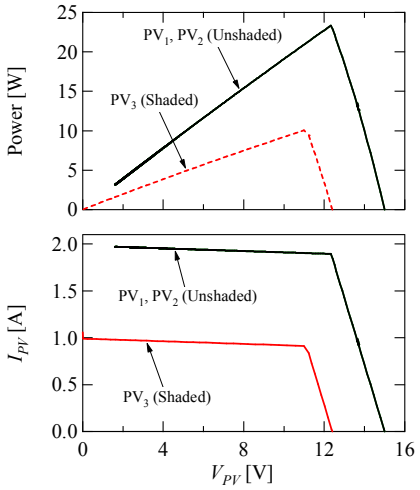

(a)

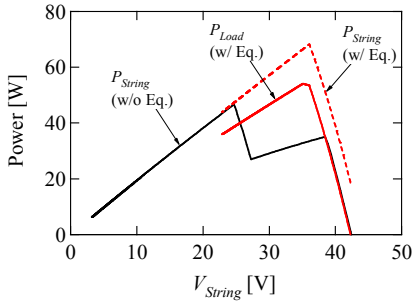

(b)

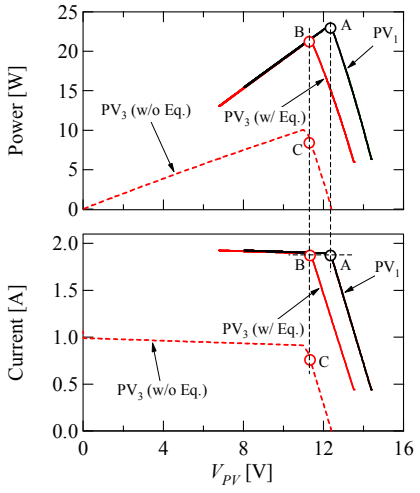

(c)

Fig. 20. Simulation results of equalization test: (a) Individual PV module characteristics used for the simulation, (b) string characteristics with/without equalization, (c) individual module characteristics with equalization.

PWM buck converter and SRVM by utilizing the square wave voltage generated across a filter inductor in the PWM buck converter for driving the SRVM. Not only can the two converters (i.e., the PWM buck converter and voltage equalizer) be integrated into a single unit but also both the switch and magnetic component counts are only one, achieving system- and circuit-level simplifications.

Fundamental operation analysis was performed, followed by the detailed analysis for the SRVM. Based on the analysis, the dc equivalent circuit of the proposed integrated converter as a whole was derived, with which simulation burden and time can be greatly mitigated.

The experimental equalization test using the prototype for three PV modules connected in series was performed emulating the partially-shaded condition, and the string characteristics with/without equalization by the integrated converter were compared. The integrated converter eliminated the local MPP, which was found when without equalization, and the available power at the load was significantly improved by the integrated converter. The simulation-based equalization test using the derived dc equivalent circuit was also performed emulating the same condition as the experiment using solar array simulators. The agreement between the experimental and simulation results verified the analysis and derived dc equivalent circuit.

REFERENCES

[1] S. Poshtkouhi, V. Palaniappan, M. Fard, and O. Trescases, "A general approach for quantifying the benefit of distributed power electronics for fine grained MPPT in photovoltaic applications using 3-D modeling," *IEEE Trans. Power Electron.*, vol. 27, no. 11, pp. 4656–4666, Nov. 2012.

[2] M. Vitelli, "On the necessity of joint adoption of both distributed maximum power point tracking and central maximum power point tracking in PV systems," *Prog. Photovolt. Res. Appl.*, vol. 22, pp. 283-299, 2014.

[3] P. S. Shenoy, K. A. Kim, B. B. Johnson, and P. T. Krein, "Differential power processing for increased energy production and reliability of photovoltaic systems," *IEEE Trans. Ind. Power Electron.*, vol. 28, no. 6, pp. 2968–2979, Jun. 2013.

[4] H. J. Bergveld, D. Büthker, C. Castello, T. Doorn, A. D. Jong, R. V. Otten, and K. D. Waal, "Module-level dc/dc conversion for photovoltaic systems: the delta-conversion concept," *IEEE Trans. Power Electron.*, vol. 28, no. 4, pp. 2005–2013, Apr. 2013.

[5] S. Qin, C.B. Barth, and R.C.N.P. Podgurski, "Enhancing microinverter energy capture with submodule differential power processing," *IEEE Trans. Power Electron.*, vol. 31, no. 5, pp. 3575–3585, May 2016.

[6] S. Qin, S.T. Cady, A.D.D. García, and R.C.N.P. Podgurski, "A distributed approach to maximum power point tracking for photovoltaic submodule differential power processing," *IEEE Trans. Power Electron.*, vol. 30, no. 4, pp. 2024–2040, Apr. 2015.

[7] R. Kadri, J. P. Gaubert, and G. Champenois, "New converter topology to improve performance of photovoltaic power generation system under shading conditions," in Proc. *Int. Conf. Power Eng. Energy Electrical Drives*, pp. 1–7, 2011.

[8] R. Kadri, J. P. Gaubert, and G. Champenois, "Centralized MPPT with string current diverter for solving the series connection problem in photovoltaic power generation system," in Proc. *Int. Conf. Power Eng. Energy Electrical Drives*, pp. 116–123, 2011.

[9] R. Giral, C.A.R. Paja, D. Gonzalez, J. Calvente, À.C. Pastpr, and L.M. Salamero, "Minimizing the effects of shadowing in a PV module by means of active voltage sharing," in Proc. *IEEE Int. Conf. Ind. Technol*, pp. 943–948, 2010.

[10] R. Giral, C. E. Carrejo, M. Vermeersh, A. J. Saavedra-Montes, and C. A. Ramos-Paja, "PV field distributed maximum power point tracking by means of an active bypass converter," in Proc. *Int. Conf. Clean Electrical Power*, pp. 94–98, 2011.

[11] L. F. L. Villa, T. P. Ho, J. C. Crebier, and B. Raison, "A power electronics equalizer application for partially shaded photovoltaic modules," IEEE Trans. Ind. Electron., vol. 60, no. 3, pp. 1179–1190, Mar. 2013.

[12] L. F. L. Villa, X. Pichon, F. S. Ardelibi, B. Raison, J. C. Crebier, and A. Labonne, "Toward the design of control algorithms for a photovoltaic

equalizer: choosing the optimal switching strategy and the duty cycle," *IEEE Trans Power Electron*., vol. 29, no. 3, pp. 1447–1460, Mar. 2014.
[13] M. Z. Ramli and Z. Salam, "A simple energy recovery scheme to harvest the energy from shaded photovoltaic modules during partial shading," *IEEE Tran. Power Electron*., vol. 29, no. 12, pp. 6458–6471, Dec. 2014.
[14] S. Poshtkouhi, A. Biswas, O. Trescases, "Dc-dc converter for high granularity sub-string MPPT in photovoltaic applications using a virtual-parallel connection," in Proc. *IEEE Applied Power Electron. Conf. Expo*., pp. 86–92, 2012.
[15] T. Shimizu, O, Hashimoto, and G. Kimura, "A novel high-performance utility-interactive photovoltaic inverter system," *IEEE Trans. Power Electron*., vol. 18, no. 2, pp. 704–711, Mar. 2003.
[16] T. Shimizu, M. Hirakata, T. Kamezawa, and H. Watanabe, "Generation control circuit for photovoltaic modules," *IEEE Trans. Power Electron*., vol. 16, no. 3, pp. 293–300, May 2001.
[17] J. T. Stauth, M. D. Seeman, and K. Kesarwani, "Resonant switched-capacitor converters for sub-module distributed photovoltaic power management," *IEEE Trans. Power Electron*., vol. 28, no. 3, pp. 1189–1198, Mar. 2013.
[18] A. H. Chang, A. T. Avestruz, and S. B. Leeb, "Capacitor-less photovoltaic cell-level power balancing using diffusion charge redistribution," *IEEE Trans. Power Electron*., vol. 30, no. 2, pp. 537–546, Feb. 2015.
[19] S. B. Yaakov, A. Blumenfeld, A. Cervera, and M. Evzelman, "Design and evaluation of a modular resonant switched capacitor equalizer for PV panels," in Proc. *IEEE Energy Conversion Cong. Expo*., pp. 4129–4136, 2012.
[20] Y. Nimni and D. Shmilovitz, "Returned energy architecture for improved photovoltaic systems efficiency," in Proc. *IEEE Int. Symp. Circuit Syst*., pp. 2191–2194, 2010.
[21] C. Olalla, D. Clement, M. Rodríguez, and D. Makisimović, "Architectures and control of submodule integrated dc-dc converters for photovoltaic applications," *IEEE Trans. Power Electron*., vol. 28, no. 6, pp. 2980–2997, Jun. 2013.
[22] C. Olalla, C. Deline, D. Clement, Y. Levron, M. Rodríguez, and D. Makisimović, "Performance of power limited differential power processing architectures in mismatched PV systems," *IEEE Trans. Power Electron*., vol. 30, no. 2, pp. 618–631, Feb. 2015.
[23] Q. Zhang, X. Sun, Y. Zhong, and M. Matui, "A novel topology for solving the partial shading problem in photovoltaic power generation system," in Proc. *IEEE Power Electron. Motion Cont. Conf*., pp. 2130–2135, 2009.
[24] J. Du, R. Xu, X. Chen, Y. Li, and J. Wu, "A novel solar panel optimizer with self-compensation for partial shadow condition," in Proc. *IEEE Applied Power Electron. Conf. Expo., APEC*, pp. 92–96, 2013.
[25] M. Uno and A. Kukita, "Single-switch voltage equalizer using multi-stacked buck-boost converters for partially-shaded photovoltaic modules," *IEEE Trans. Power Electron*., vol. 30, no. 6, pp. 3091–3105, Jun. 2015.
[26] M. Uno and A. Kukita, "Current sensorless equalization strategy for a single-switch voltage equalizer using multistacked buck–boost converters for photovoltaic modules under partial shading," *IEEE Trans. Ind. Appl*., vol. 53, no. 1, pp. 420–429, Jan./Feb. 2017.
[27] M. Uno and A. Kukita, "Two-switch voltage equalizer using an LLC resonant inverter and voltage multiplier for partially-shaded series-connected photovoltaic modules," *IEEE Trans. Ind. Appl*., vol. 51, no. 2, pp. 1587–1601, Mar./Apr. 2015.
[28] M. Uno and A. Kukita, "Single-switch PWM converter integrating voltage equalizer for photovoltaic modules under partial shading" in Proc. *IEEE Int. Power Electron. Conf, IPEC-Hiroshima, ECCE Asia*, pp. 2351–2358, May. 2014.
[29] M. Uno and A. Kukita, "Single-switch single-magnetic PWM converter integrating voltage equalizer for series-connected photovoltaic modules under partial shading" in Proc. *IEEE Energy Conversion Cong. Expo., ECCE*, pp. 5618–5625, Sep. 2014.
[30] TDK. (2010, Sep.) LLC Resonant Power Transformers. [Online]. available: http://www.ic-contract.ru/images/pdf/TDK/e636_srx.pdf#search='TDK +LLC+transforme
[31] S. M. MacAlpine, R. W. Erickson, and M. J. Brandemuehl, "Characterization of power optimizer potential to increase energy capture in photovoltaic systems operating under nonuiform conditions," *IEEE Trans. Power Electron*., vol. 28, no. 6, pp. 2936–2945, Jun. 2013.

Masatoshi Uno (M'06) was born in Japan in 1979. He received the B.E. degree in electronics engineering and the M.E. degree in electrical engineering from Doshisha University, Kyoto, Japan, and the Ph.D. degree in space and astronautical science from the Graduate University for Advanced Studies, Hayama, Japan, in 2002, 2004, and 2012, respectively. In 2004, he joined the Japan Aerospace Exploration Agency, Sagamihara, Japan, where he developed spacecraft power systems including battery, photovoltaic, and fuel cell systems. In 2014, he joined the Department of Electrical and Electronics Engineering, Ibaraki University, Ibaraki, Japan, where he is currently an Associate Professor of Electrical Engineering. His research interests include switching power converters, cell equalizers, life evaluation for supercapacitors and lithium-ion batteries, and development of fuel cell systems. Dr. Uno is a member of the Institute of Electrical Engineers of Japan (IEEJ) and the Institute of Electronics, Information, and Communication Engineers (IEICE).

M. Uno is a member of the Institute of Electrical Engineering of Japan (IEEJ), and the Institute of Electronics, Information and Communication Engineers (IEICE).

Akio Kukita was born in Japan in 1967. He received the B.E. degree in physics from Chuo University, Japan, in 1993.

From 1993 to 1996 and 1996 to 2008, he was with SEIKO Holdings Corporation and Ebara Corporation, respectively. Since 2008, he has been with Japan Aerospace Exploration Agency as a senior engineer. His recent work has focused on the development of spacecraft power systems.